Electronic Supplementary Information

Nanostructured Materials for Photodynamic Therapy: Synthesis, Characterization and *in vitro* Activity

María E. Alea-Reyes,[a,b] Mafalda Rodrigues,[a,b] Albert Serrà,[b,c] Margarita Mora,[d] Maria L. Sagristá,[d] Asensio González,[a] Sara Durán,[e] Marta Duch,[e] José Antonio Plaza,[e] Elisa Vallés,[b,c] David A. Russell,[f] and Lluïsa Pérez-García[a,b]‡*

a. Departament de Farmacologia, Toxicologia i Química Terapèutica, Universitat de Barcelona, Avda. Joan XXIII 27-31, 08028 Barcelona, Spain.

E-mail: mlperez@ub.edu

b. Institut de Nanociència i Nanotecnologia UB (IN2UB), Universitat de Barcelona, Avda. Joan XXIII 27-31, 08028 Barcelona, Spain.

c. Ge-CPN, Departament de Química Física, Universitat de Barcelona, C/ Martí i Franquès 1, 08028 Barcelona, Spain.

d. Departament de Bioquímica i Biologia Molecular, Facultat de Biologia, Universitat de Barcelona, Avda. Diagonal 643, 08028 Barcelona, Spain.

e. Instituto de Microelectrónica de Barcelona (IMB-CNM (CSIC)), Campus UAB, 08193, Cerdanyola, Barcelona, Spain).

f. School of Chemistry, University of East Anglia, Norwich Research Park, Norwich, Norfolk, NR4 7TJ, UK.

‡ Present address: School of Pharmacy, The University of Nottingham, University Park, Nottingham NG72RD, England, UK.

Table of Contents

1) Synthesis and characterization of the porphyrin derivatives

$TPPNH_2$ and its Zn (II) derivative **$ZnTPPNH_2$** are the key scaffolds to be derivatized with sulphur containing groups linkable to gold, which was accomplished by reaction with lipoic acid to give **ATPP-LA** and **ZnATPP-LA**, respectively (Scheme S1).

The synthesis of **$TPPNH_2$**, was performed according to modifications of methods previously described in the literature[1–3] (see Scheme S1). In the synthesis of **$ZnTPPNH_2$**[4] an excess of zinc acetate was added to a solution of **$TPPNH_2$** in $MeOH/CHCl_3$. Subsequently both porphyrins (**$TPPNH_2$** and **$ZnTPPNH_2$**) were treated with one equivalent of lipoic acid (LA) in presence of DCC and HOBT to give porphyrins **ATPP-LA_1** and **ZnATPP-LA** in good yields (87% and 93% respectively) as we can see in Scheme 1.

Unexpectedly, the coupling of the lipoic acid to **$TPPNH_2$** afforded a product where oxidation of the sulphur atoms had occurred, as indicated by Mass Spectrometry and Elemental Analysis. The oxidation of disulphide groups has been reported in literature.[5,6] Due to the oxidation of the disulphide group in the product **ATPP-LA_1**, an additional reduction step using $NaBH_4$ was necessary to obtain **ATPP-LA** (Scheme S2). All porphyrins synthesized had a high degree of purity.

5,10,15,20-tetrakis(4-biphenyl)porphyrin (TPP)[1] (Scheme S1)

TPP was obtained in 70% yield by refluxing equivalent amounts of pyrrole and benzaldehyde in propionic acid, following the Adler-Longo method.[1]

5-(4-nitrophenyl)-10,15,20-triphenylporphyrin ($TPPNO_2$)[2] (Scheme S1)

TPP (0.5 g) was added to a solution of trichloroacetic acid (15 g) in DCM (50 mL), and then concentrated HNO_3 (156 µl, 65%) was added dropwise, using an external ice bath. The mixture was stirred for 3 min. The reaction was quenched with water (100 mL), and the mixture was neutralized with ammonium hydroxide (28%) to pH =7 (the color of the reaction changed from green to brown). The product was extracted with DCM (2 x 100 mL), and the organic layer was washed with water (3 x 50 mL) and dried over sodium sulfate anhydrous and then concentrated under vacuum. The residue was purified on aluminum oxide basic using for elution chloroform to give **$TPPNO_2$** as a brown solid (340 mg, 65%): m.p.> 300 °C, rf = 0.68 in chloroform. UV-vis λmax (DCM)/nm 421, 518, 552, 592 and 648. ^{1}H-NMR (400 MHz, $CDCl_3$; 25 °C): δ ppm= -2.75 (s, 2H, -NH), 7.81-7.76 (m, 9H, Ar-H), 8.40-8.21 (m, 6H, Ar-H), 8.42 (d, *J*= 3.8 Hz, 2H, nitrophenyl), 8.64 (d, *J* = 3.8 Hz, 2H, nitrophenyl), 8.74 (d, *J* = 4.4 Hz, 2H, β-pyrrole), 8.87 (s, 4H, β-pyrrole), 8.90 (d, *J* = 4.4 Hz, 2H, β-pyrrole). MALDI-ToF-MS m/z (%)= 659.1 (100) $[M]^+$.

5-(4-Aminophenyl)-10,15,20-triphenylporphyrin ($TPPNH_2$)[3] (Scheme S1)

$TPPNO_2$ could be easily reduced to the corresponding amino-porphyrin (**$TPPNH_2$**) by the Kruper method with a good yield of 98%.

Zn(II) 5-(4-Aminophenyl)-10,15,20-triphenylporphyrin ($ZnTPPNH_2$)

In the synthesis of $ZnTPPNH_2$[4] (Scheme 1), an excess of zinc acetate was added to a solution of $TPPNH_2$ in $MeOH/CHCl_3$. The reaction was monitored by UV-visible absorption spectroscopy: the porphyrins present a characteristic absorption spectrum consisting of an intense Soret band and 4 or 2 less intense so-called Q bands. In the case of the $TPPNH_2$, the absorption spectrum shows four Q bands (Figure S3) that upon coordination with Zn (II), are replaced by two Q bands (Figure S4) due to the presence of Zn in the core, thus indicating the formation of $ZnTPPNH_2$.

Zn (ll) 5-(4-Aminophenyl)-10,15,20-triphenylporphyrin (ZnTPPNH$_2$)[4]

A solution of **TPPNH$_2$** (63 mg, 0.1 mmol) in $CHCl_3$ (30 mL) was heated to reflux under an argon atmosphere. A solution of $Zn(OAc)_2 \cdot 2H_2O$ (417 mg, 1.8 mmol) in MeOH (15 mL) was added dropwise, and the whole was refluxed for 24 h. The mixture was washed with a saturated solution of 5% $NaHCO_3$ (50 mL). Then the product was extracted with DCM (2 x 50 mL), and the organic layer was washed with water (2 x 50 mL) and dried over sodium sulfate (99%) and the organic layer was evaporated under reduced pressure and the crude product purified by column chromatography (SiO_2, DCM) to afford a purple solid (110 mg, 84%): m.p. > 300 °C, rf = 0.47 in chloroform. UV-vis (DCM) λmax 429, 556, 598 nm ^{1}H-NMR (400 MHz, $CDCl_3$, 25 °C): δ ppm= 3.89 (s, 2H, amino), 7.01 (d, *J* = 8.0 Hz, 2H, 4-aminophenyl), 7.76-7.74 (m, 9H, Ar-H), 7.97 (d, *J* = 8.2 Hz, 2H, 4-aminophenyl), 8.23-8.21 (m, 6H, Ar-H), 8.93 (s, 6H, β-pyrrole), 9.04 (d, 2H, *J* = 4.5 Hz, β-pyrrole). MALDI-ToF-MS: m/z (%)= 691.1 (100) $[M]^+$.

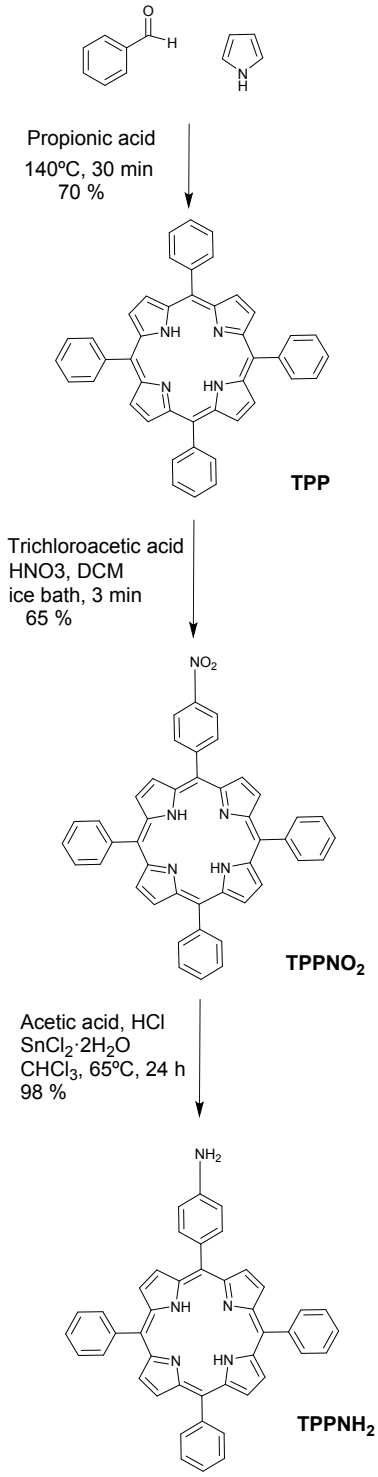

Scheme S1. Synthesis of the porphyrins **TPP**, **TPPNO$_2$** and **TPPNH$_2$**

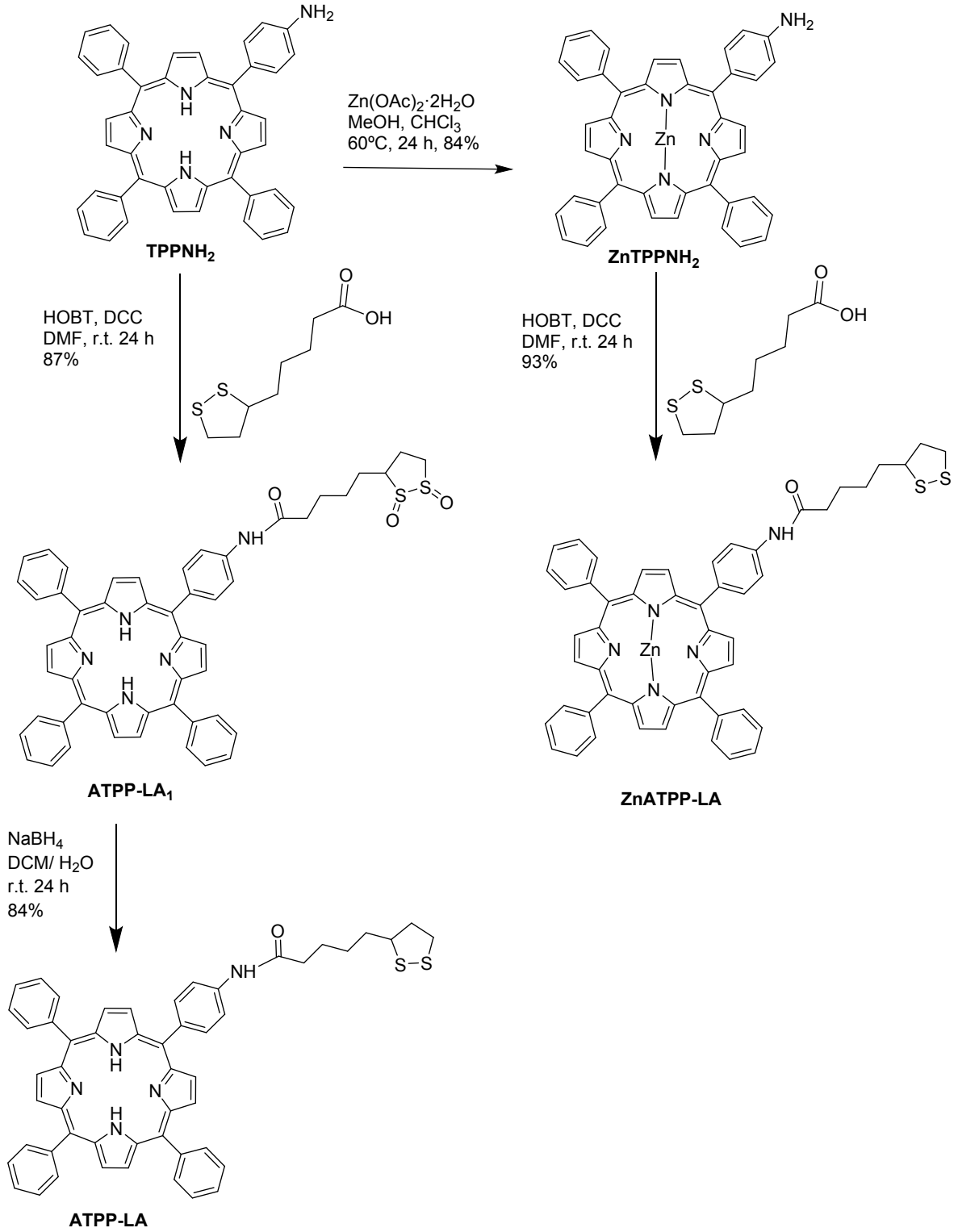

Scheme S2. Synthesis of the porphyrins **ATPP-LA$_1$**, **ATPP-LA** and **ZnATPP-LA**.

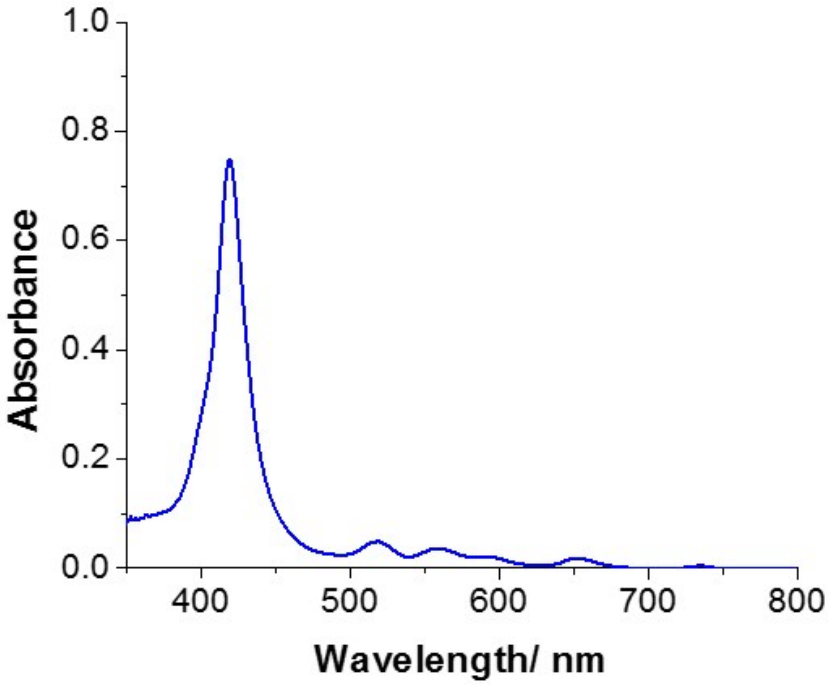

Fig S1. UV-visible absorption spectra of the **TPPNH$_2$** (3 μM) recorded in DCM.

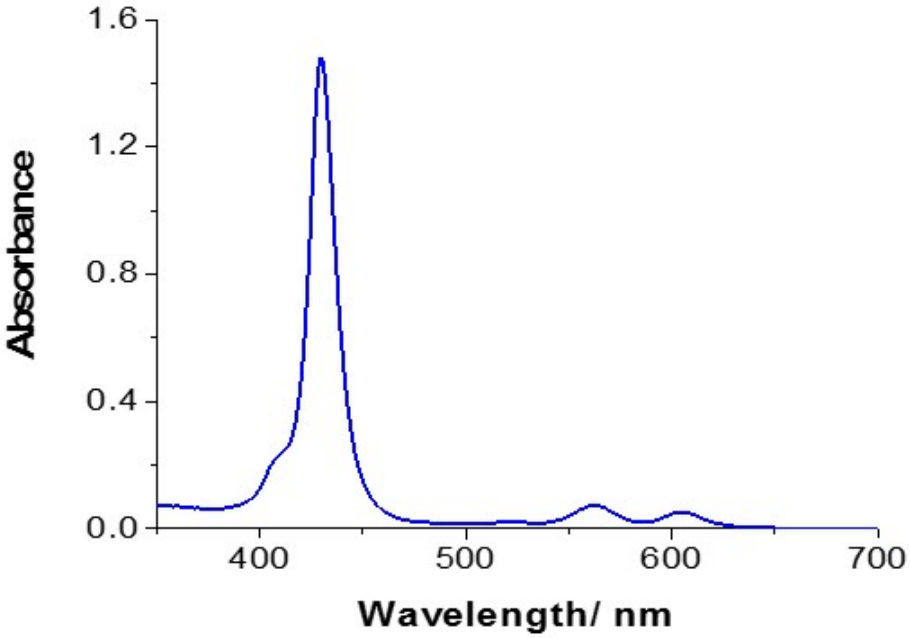

Fig S2. UV-visible absorption spectra of the **ZnTPPNH$_2$** (5 μM) recorded in DCM.

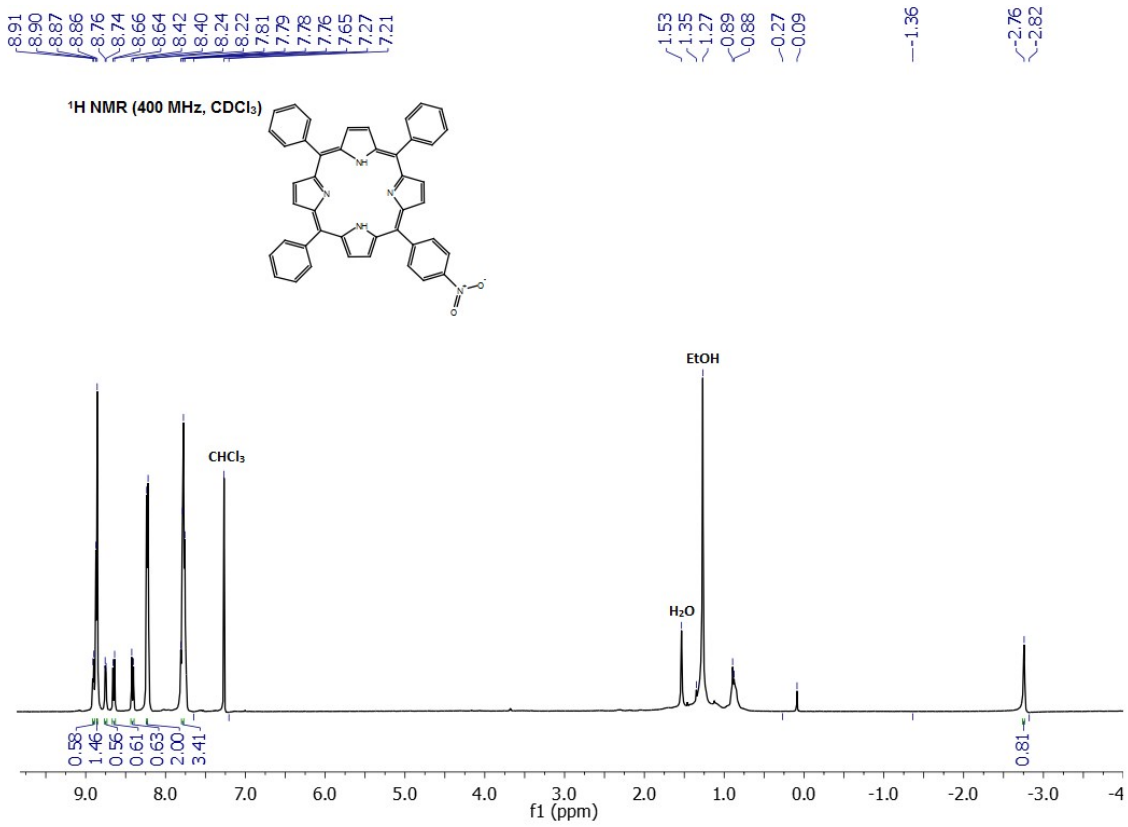

Fig S3. ^{1}H-NMR spectrum of **TPPNO$_2$** recorded in $CDCl_3$ at 400 MHz.

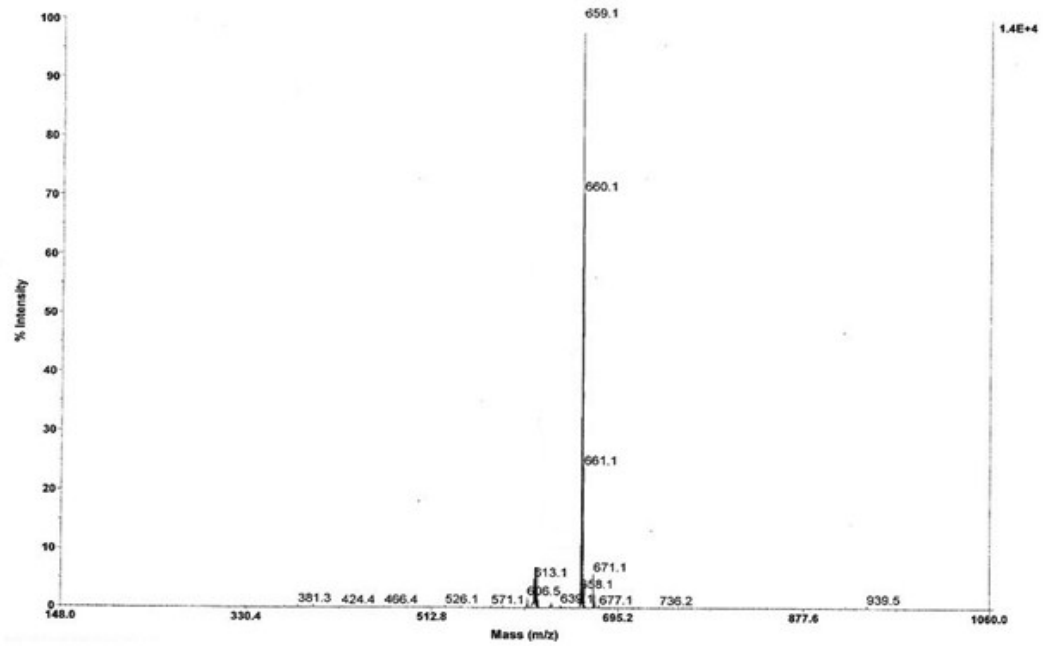

Fig S4. MALDI-ToF -MS (m/z) spectrum of **TPPNO$_2$** with DHB as matrix.

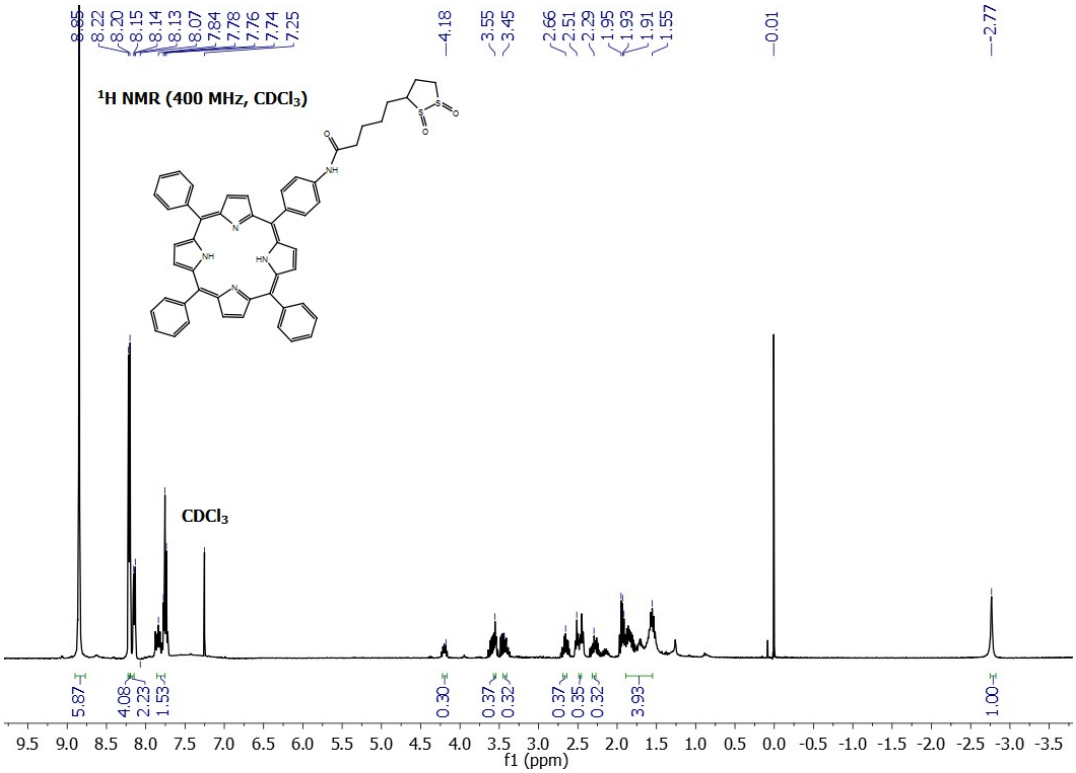

Fig S5. ^{1}H-NMR spectrum of **ATPP-LA$_1$** recorded in $CDCl_3$ at 400 MHz.

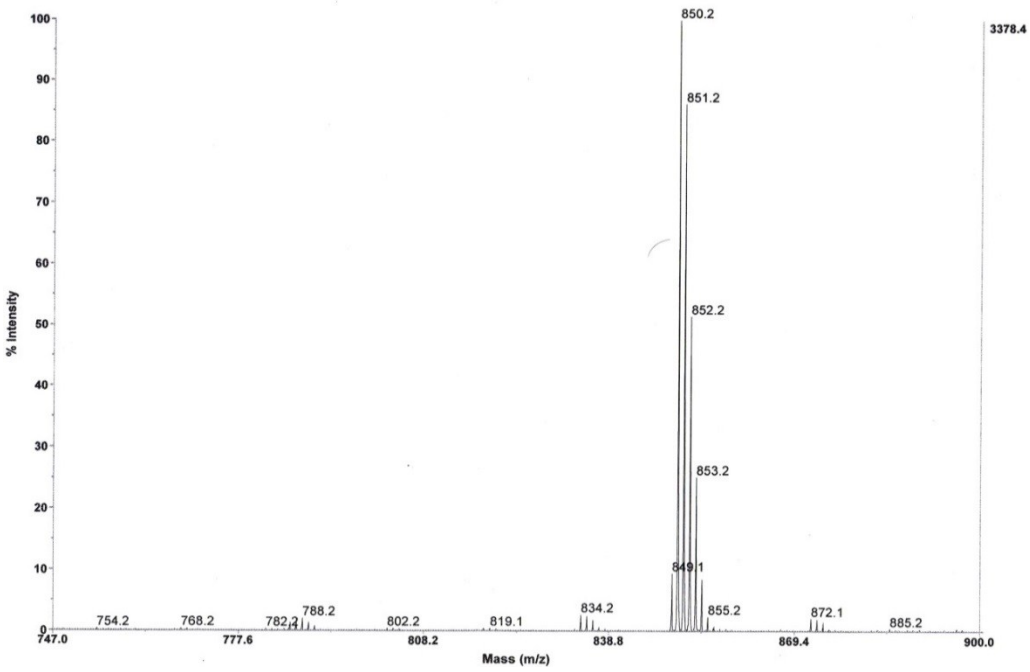

Fig S6. MALDI-ToF -MS (m/z) spectrum of **ATPP-LA$_1$** with DHB as matrix.

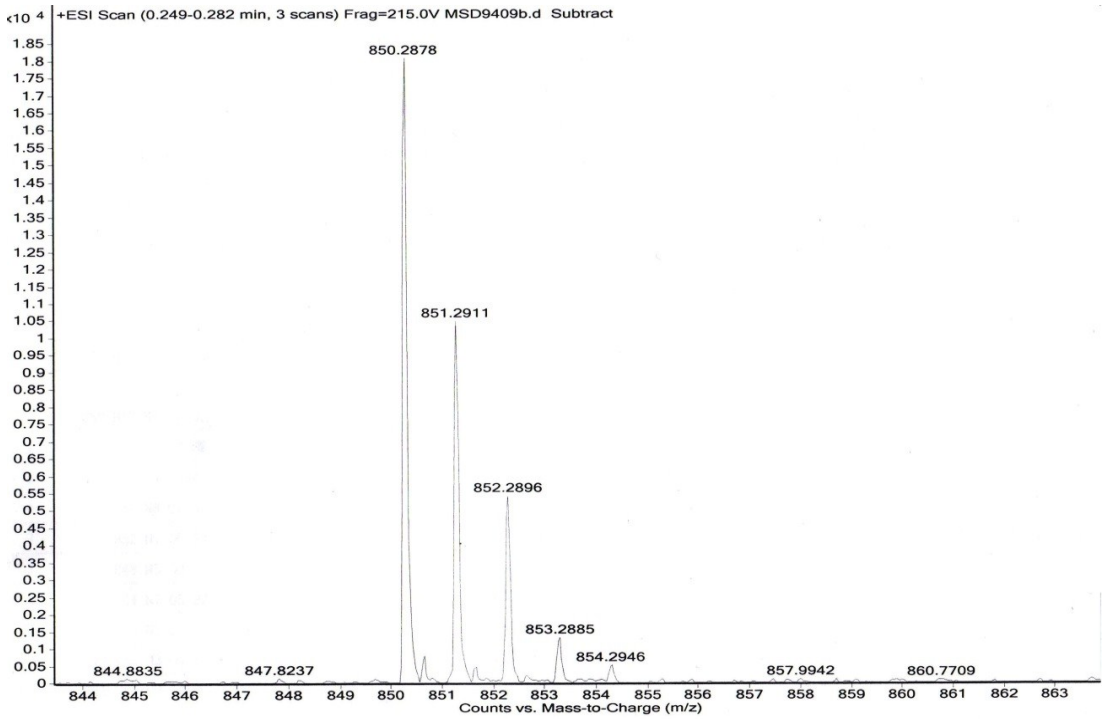

Fig S7. HMRS-ESI spectrum (m/z) spectrum of **ATPP-LA$_1$**.

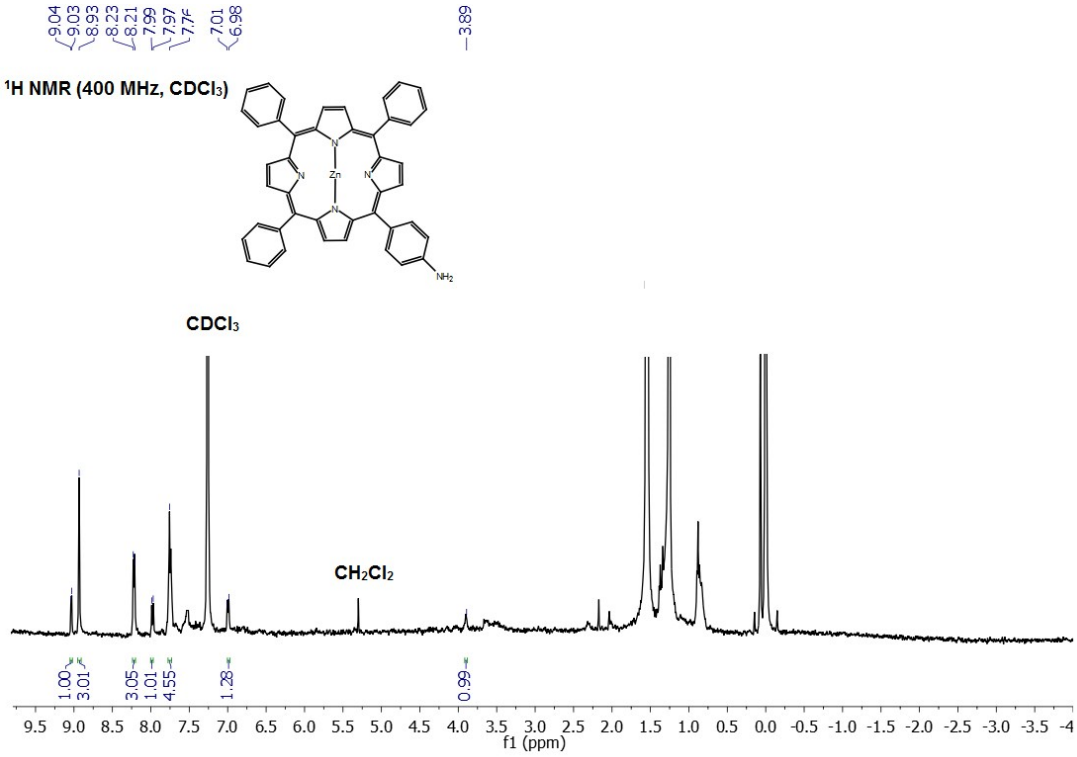

Fig S8. ^{1}H-NMR spectrum of **ZnTPPNH$_2$** recorded in $CDCl_3$ at 400 MHz.

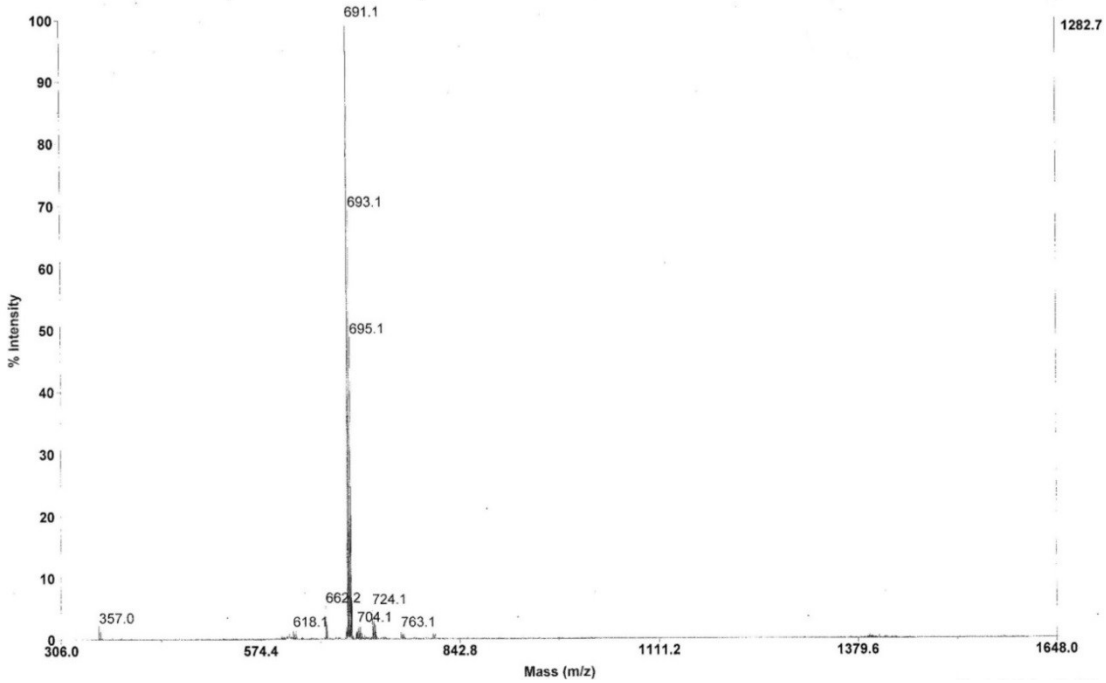

Fig S9. MALDI-ToF -MS (m/z) spectrum of **ZnTPPNH$_2$** with DHB as matrix.

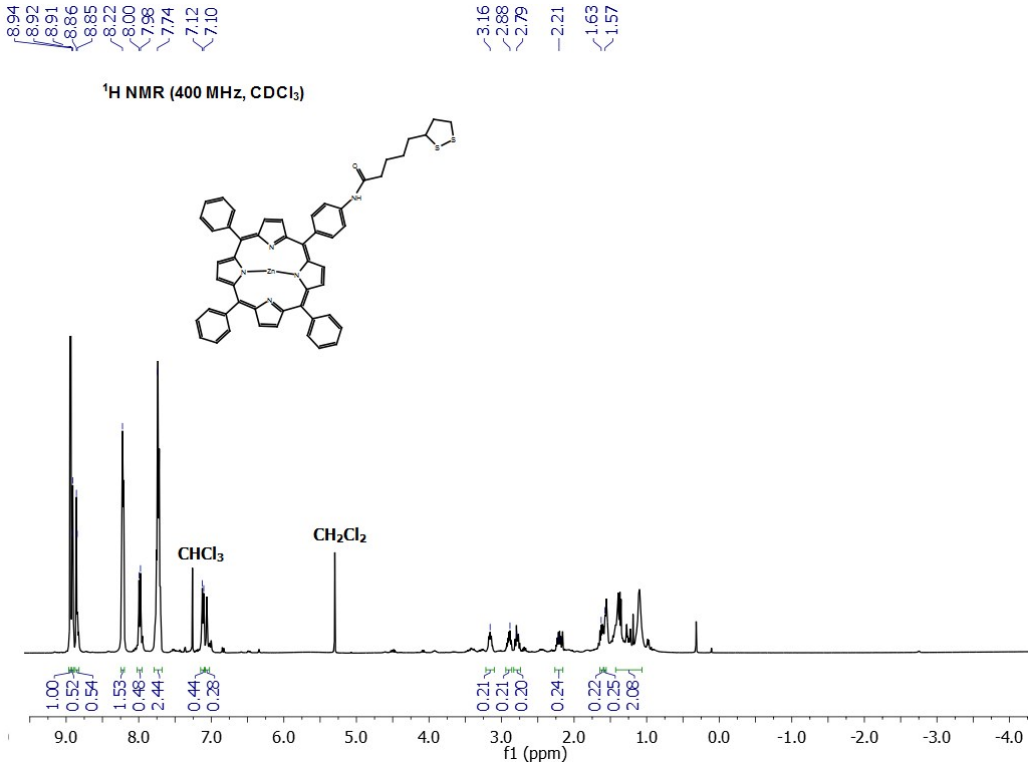

Fig S10. ^{1}H-NMR spectrum of **ZnATPP-LA** recorded in $CDCl_3$ at 400 MHz.

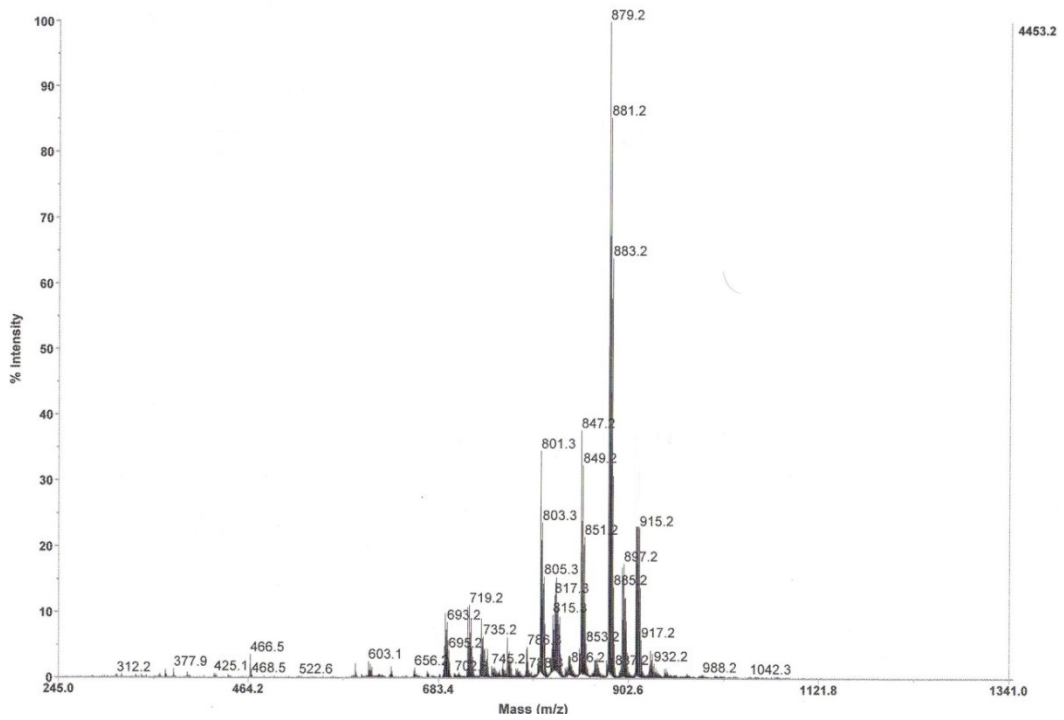

Fig S11. MALDI-ToF -MS (m/z) spectrum of **ZnATPP-LA** with DHB as matrix.

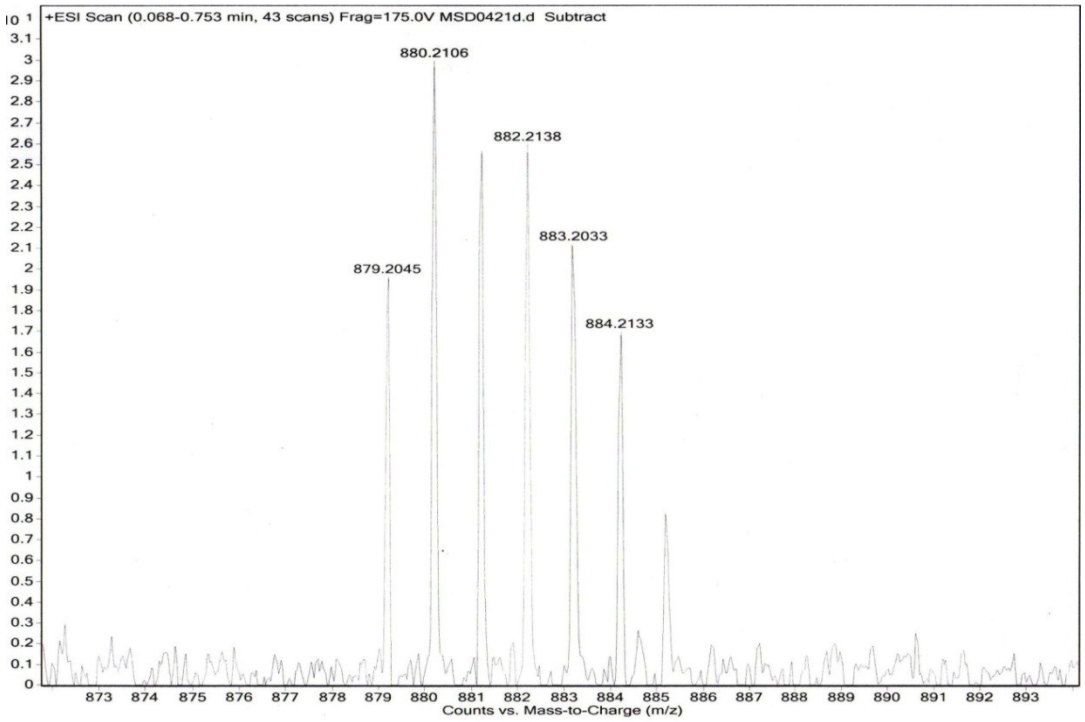

Fig S12. HMRS-ESI spectrum (m/z) spectrum of **ZnATPP-LA**.

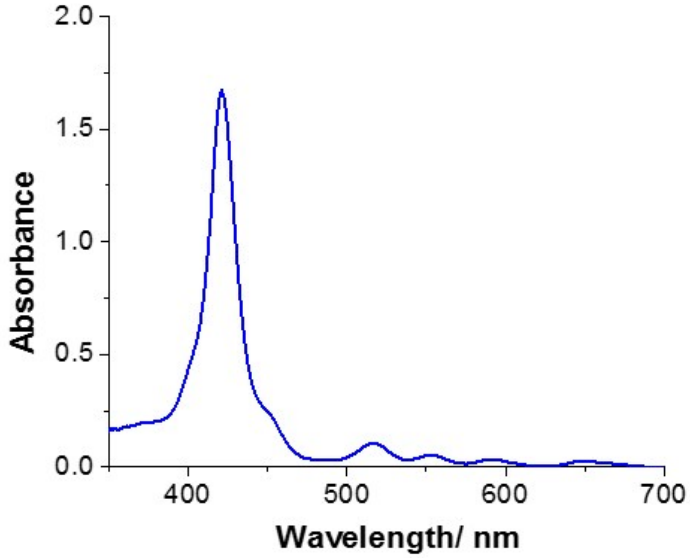

Fig S13. UV-visible absorption spectra of **TPPNO$_2$** (5 μM) recorded in DCM.

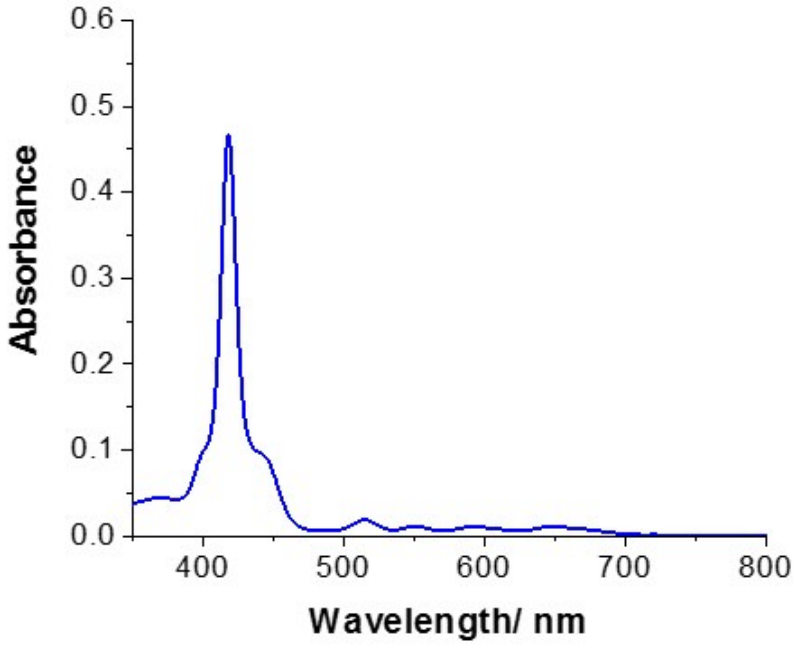

Fig S14. UV-visible absorption spectra of the **ATPP-LA$_1$** (2 μM) recorded in DCM.

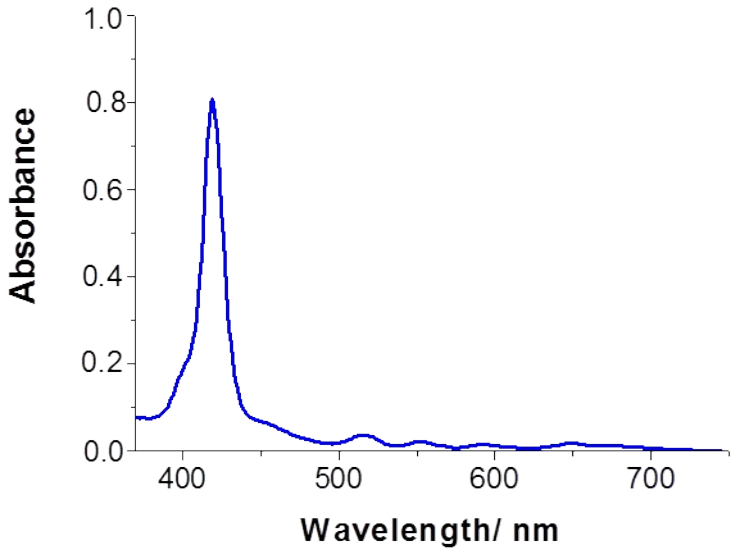

Fig S15. UV-visible absorption spectra of the **ATPP-LA** (10 μM) recorded in DCM.

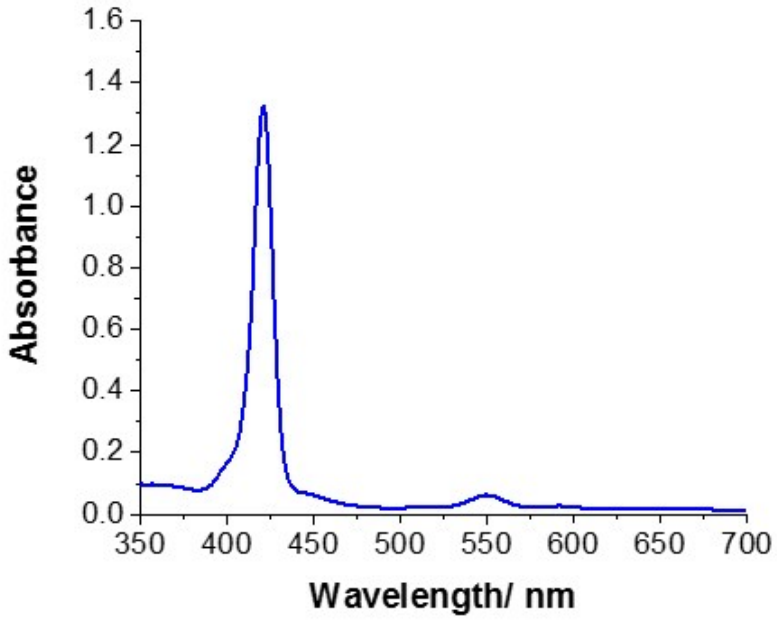

Fig S16. UV-visible absorption spectra of the **ZnATPP-LA** (10 μM) recorded in DCM.

2) Fabrication of gold coated nanorods and bifunctional microparticles

2.1. Gold coated nanorods

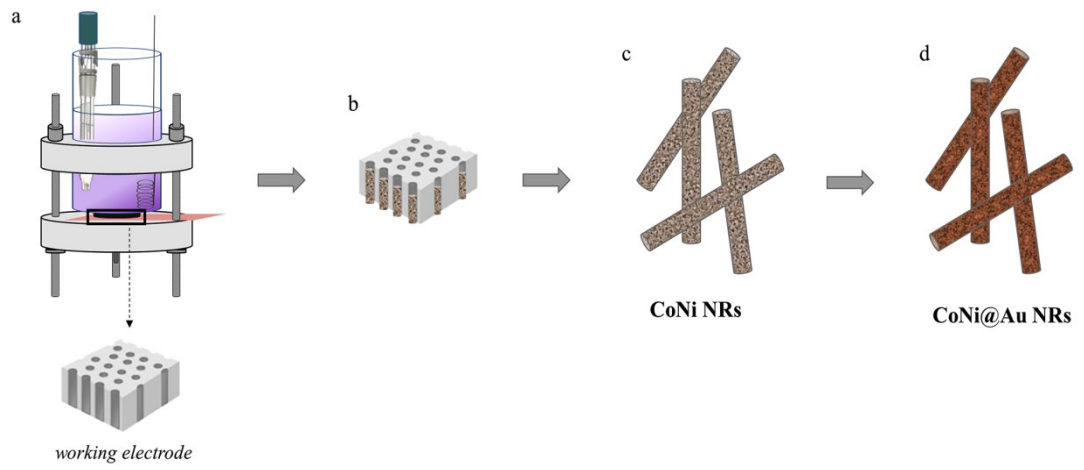

Fig S17. Schematic representation of the fabrication process of the CoNi@Au NRs. (a) Electrochemical synthesis of CoNi NRs in the interior of a gold-coated polycarbonate membrane (100 nm of nominal pore's diameter) by means of potentiostatic method. (b) CoNi NRs grown in the channels of the polycarbonate membrane. (c) Removing of the NRs by dissolution of both gold coating and polycarbonate membrane. (d) Formation of a gold shell in the surface of the CoNi NRs by means of galvanic displacement procedure.[7]

2.2. Bifunctional microparticles

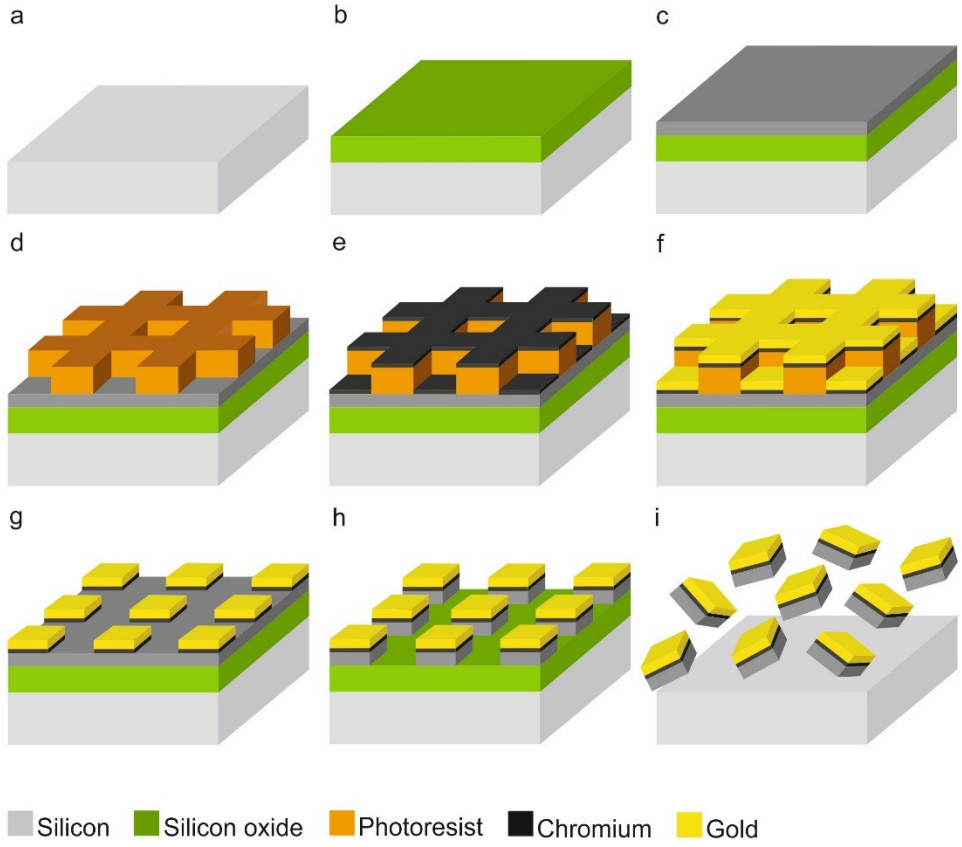

Fig S18. Fabrication process of the Polysilicon–Chromium–Gold chips.

a) Chips were fabricated using a 100 mm-diameter silicon wafer as a main substrate. b) A 1 µm silicon oxide layer was deposited as a sacrificial layer by plasma enhanced chemical vapor deposition process (PECVD). c) A 400 nm-thick polysilicon layer was deposited as a first device material by low pressure chemical vapour deposition process (LPCVD). d) A photoresist layer was spun and exposed to UV light to pattern the devices. e) Next, a chromium layer of 30 nm-thick was deposited by a sputtering process to improve the adherence between the polysilicon and gold main device layers. f) Then, a 100 nm-thick gold layer was also sputtered as a second device material. g) A lift-off process was performed to remove the chromium and gold layers from the undesired areas. h) Subsequently, the polysilicon layer was patterned using the chromium and gold layers as a mask. i) Finally, the silicon oxide sacrificial layer was etched by a 49% HF vapors to release the Polysilicon–Chromium–Gold chips and collected in ethanol.[8]

3) Characterization of the different vehicles loaded with porphyrins

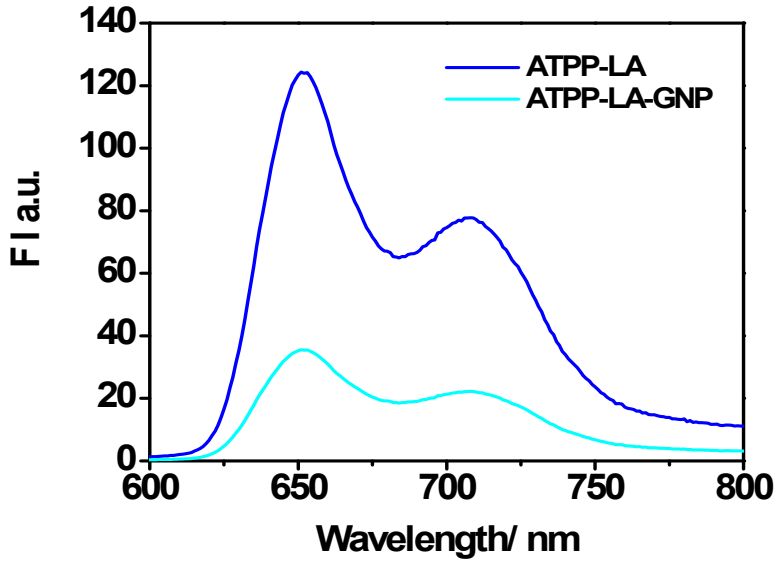

Fig S19. Fluorescence emission spectra (excitation at 590 nm) of **ATPP-LA** (0.01 mg mL^{-1}) in $CHCl_3$ and the **ATPP-LA-GNP** (0.3 mg mL^{-1}) recorded in water at 25°C.

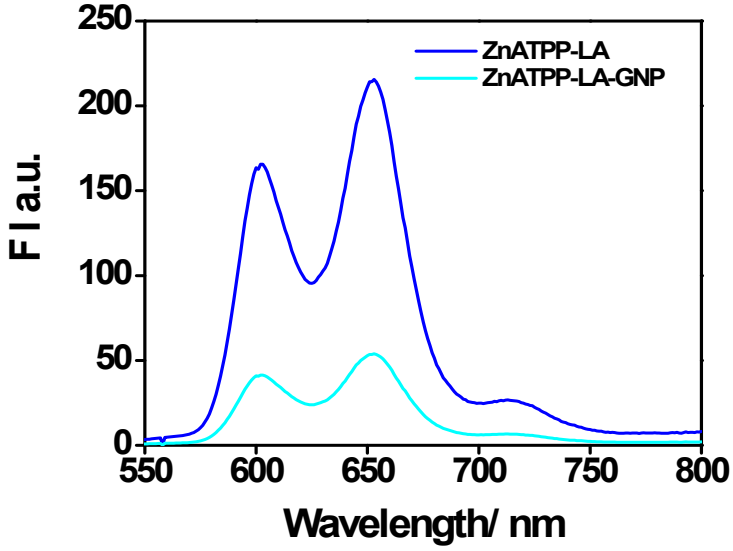

Fig S20. Fluorescence emission spectra (excitation at 550 nm) of **ZnATPP-LA** (0.02 mg mL^{-1}) in $CHCl_3$ and the **ZnATPP-LAGNP** (0.2 mg mL^{-1}) recorded in water at 25°C.

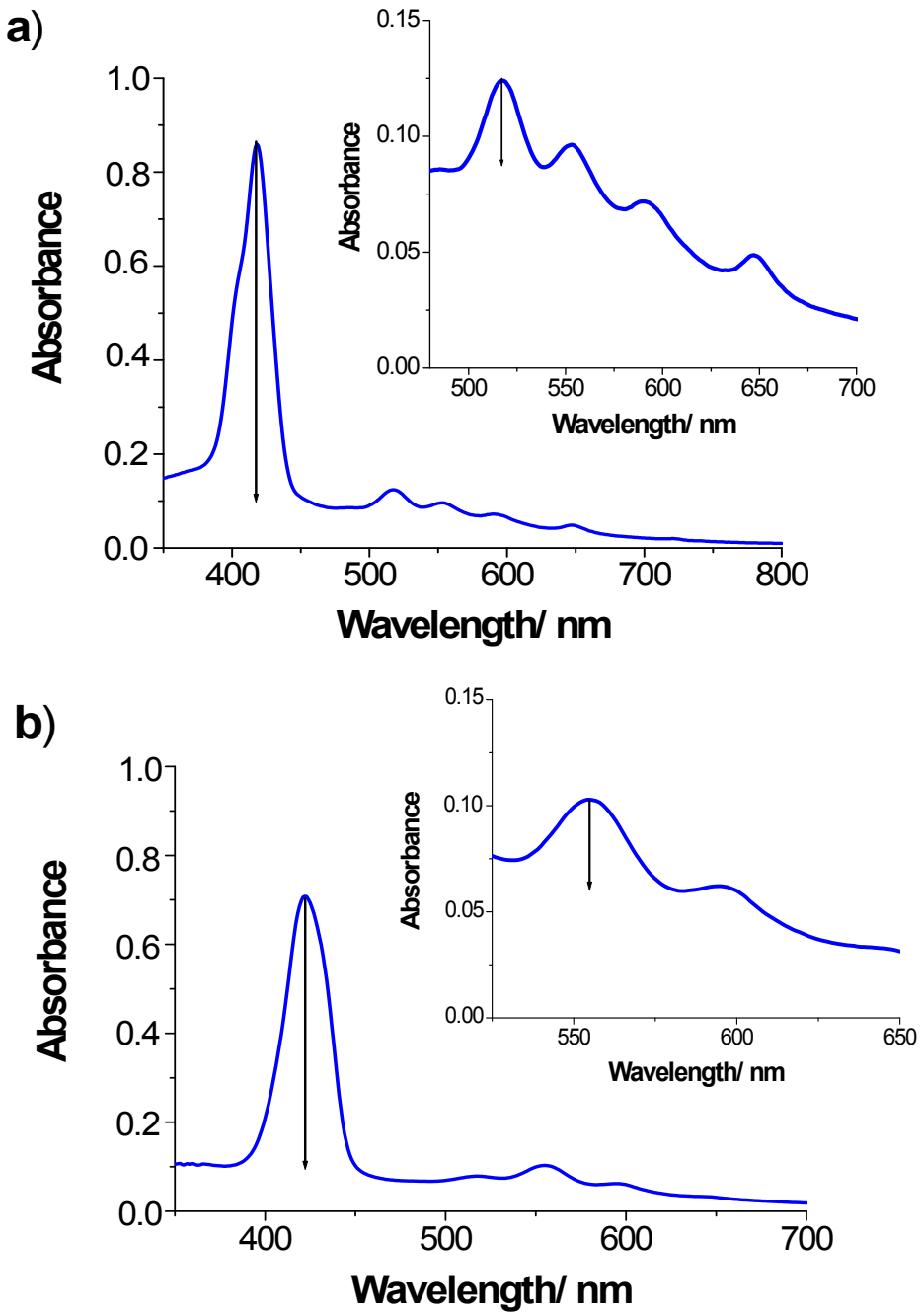

Fig S21. UV-vis absorption spectra of: a) **ATPP-LA-GNP** (0.11 mg mL^{-1}) recorded in water and b) **ZnATPP-LA-GNP** (0.18 mg mL^{-1}) recorded in water. Inserts: magnification of the corresponding Q band region.

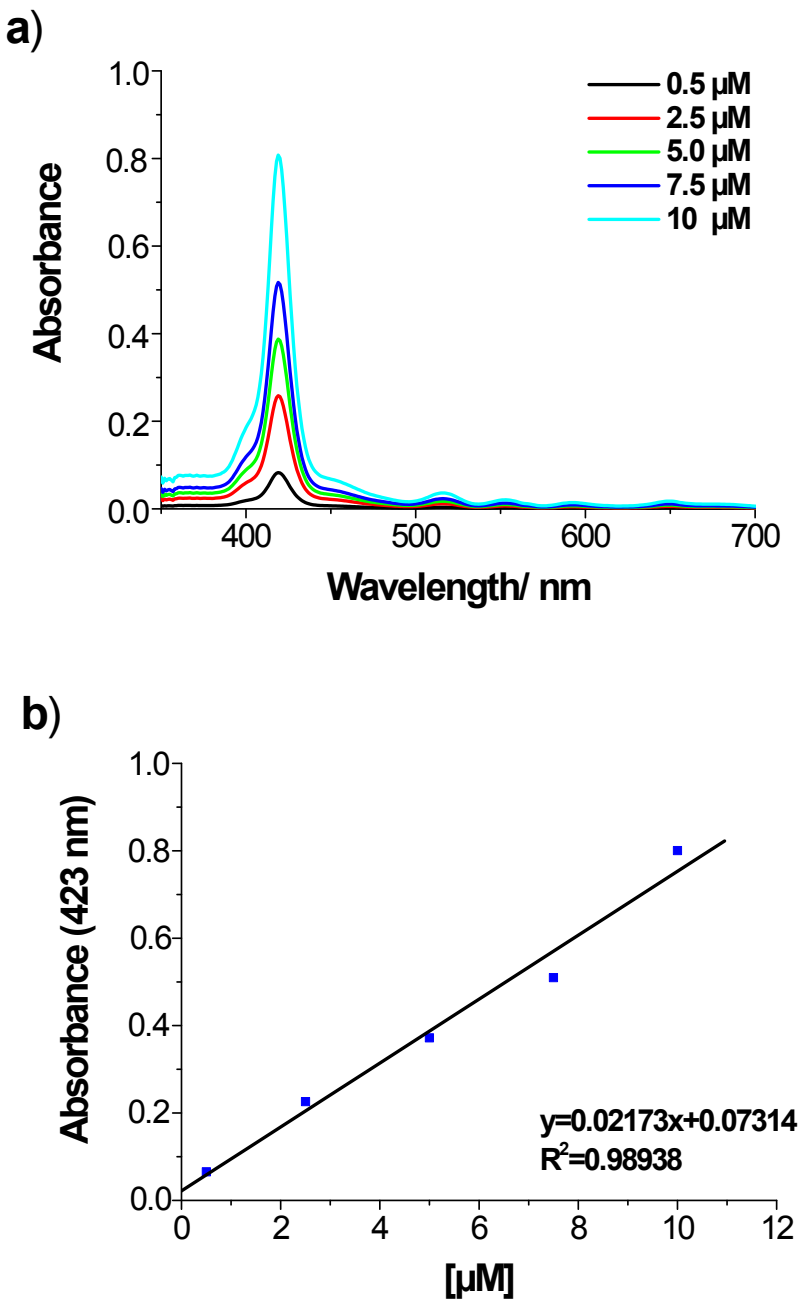

Fig S22. a) UV-vis absorption spectra of **ATPP-LA** at different concentrations (0.5-10 μM) in DCM and b) corresponding calibration curve.

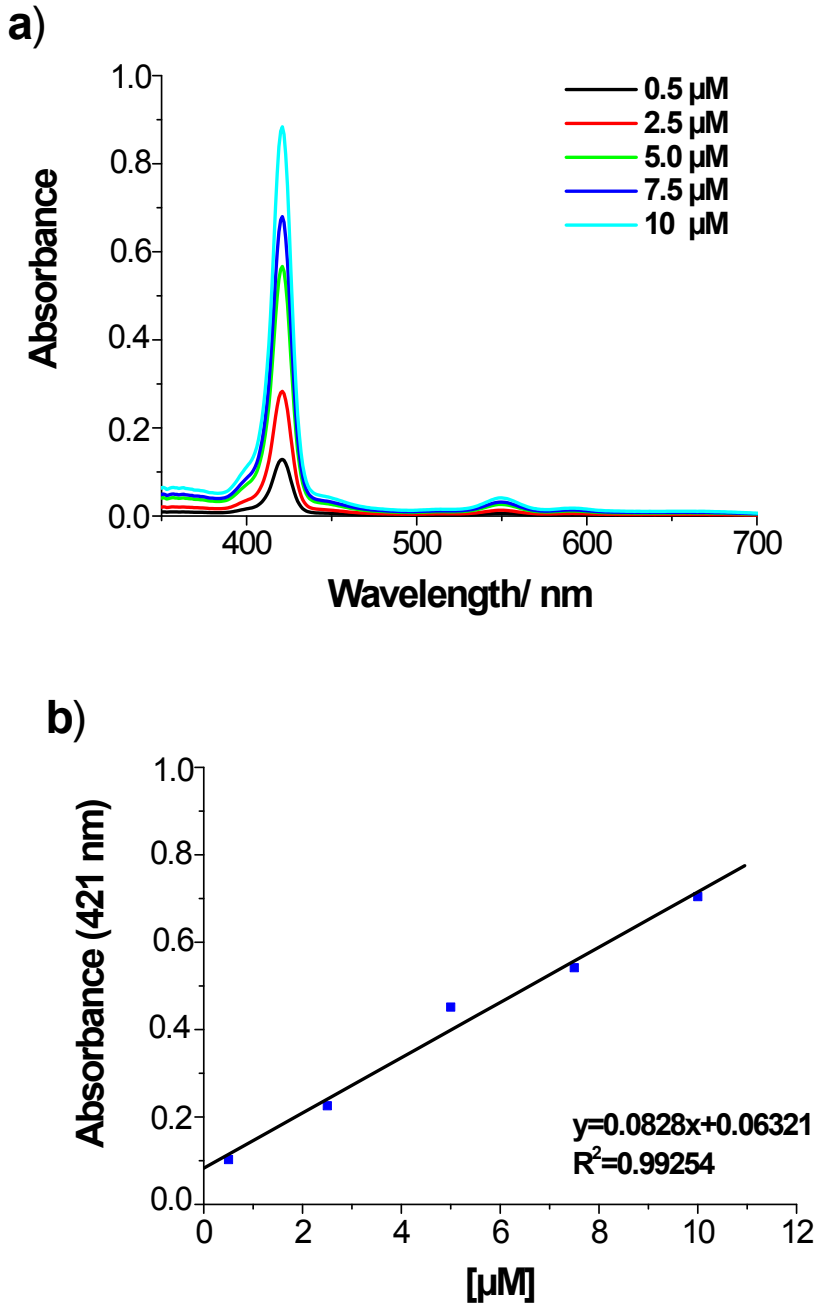

Fig S23. a) UV-vis absorption spectra of **ZnATPP-LA** at different concentrations (0.5-10 μM) in DCM and b) corresponding calibration curve.

Table S1. Calculation of number of molecules of porphyrin/GNP, with data used for the calculation

Porphyrin[a]	Soret band (nm)	Abs Soret band	Abs 480 nm	Normalized Abs[c]	ε (M^{-1} cm^{-1})	[porphyrin] (M)
ATPP-LA	422	0.7079	0.0684	0.6394	2.17×10^{4}	2.94×10^{-5}
ZnATPP-LA	418	0.8598	0.0857	0.7740	8.28×10^{4}	9.35×10^{-6}

GNP[a]	Abs_{SPR}	$Abs_{450\ nm}$	d(nm)[b]	ε (M^{-1} cm^{-1})	[GNP] (M)	Molecules of porphyrin/GNP
ATPP-LA-GNP	0.1226	0.1084	10	6.15×10^{7}	1.76×10^{-9}	1.67×10^{4}
ZnATPP-LAGNP	0.2057	0.2047	9.5	6.15×10^{7}	3.33×10^{-9}	2.81×10^{3}

[a] Absorbance peaks and values were obtained from the UV-visible absorbance spectra of free porphyrins and GNP.

[b] Diameter obtained by TEM.

[c] Normalization of the Soret Band peak absorbance of the porphyrin was applied because of the influence on the spectra of the GNP SPR peak.

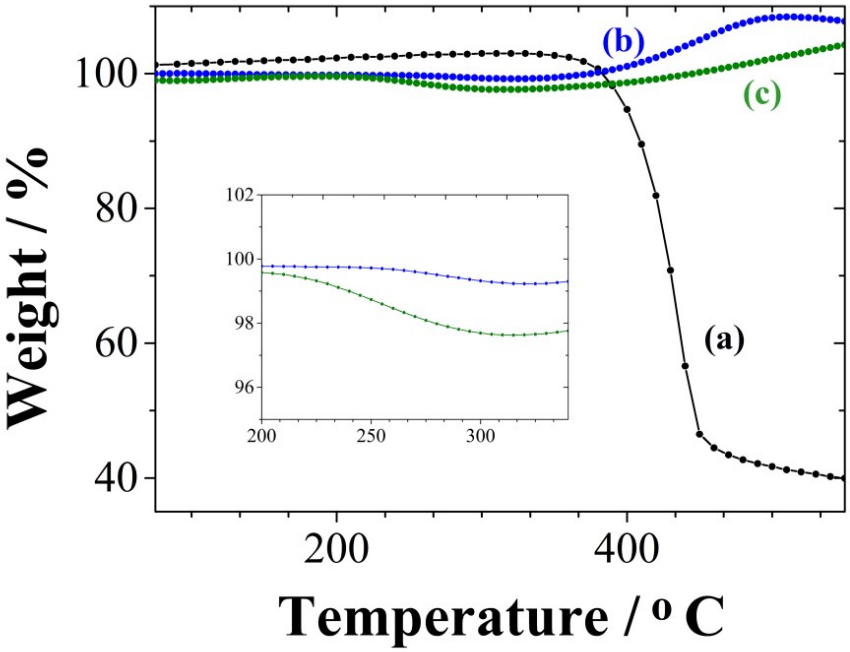

Fig S24. Thermogravimetric curves of (a) ATPP-LA, (b) ATPP-LA-NR and (c) ZnATPP-LA-NR under nitrogen atmosphere (N_2 flow: 50 mL min^{-1}) for 1 mg of each sample.

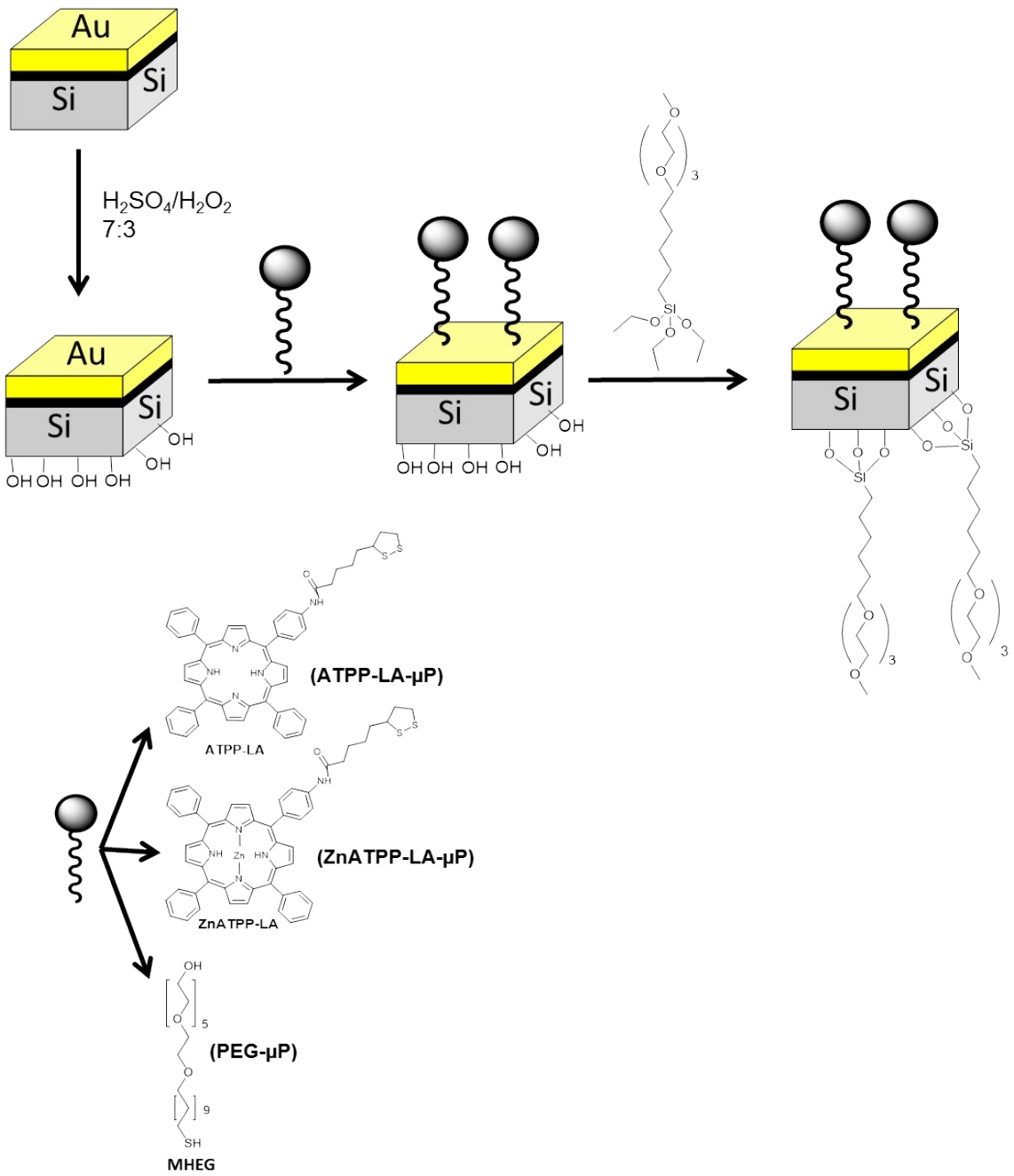

Scheme S3. Functionalization of the bifunctional microparticles: first, the microparticles are treated with piranha solution (H_2SO_4/H_2O_2 7:3) to clean organic material from the surface and also to activate the polysilicon surface. Then, the sulfur-containing molecule (**ATTP-LA**, **ZnATPP-LA** or MHEG) were added to form the monolayer on the gold surface. Afterwards, the silane containing PEG groups is added to form the monolayer on the polysilicon surface.

4) Singlet oxygen production

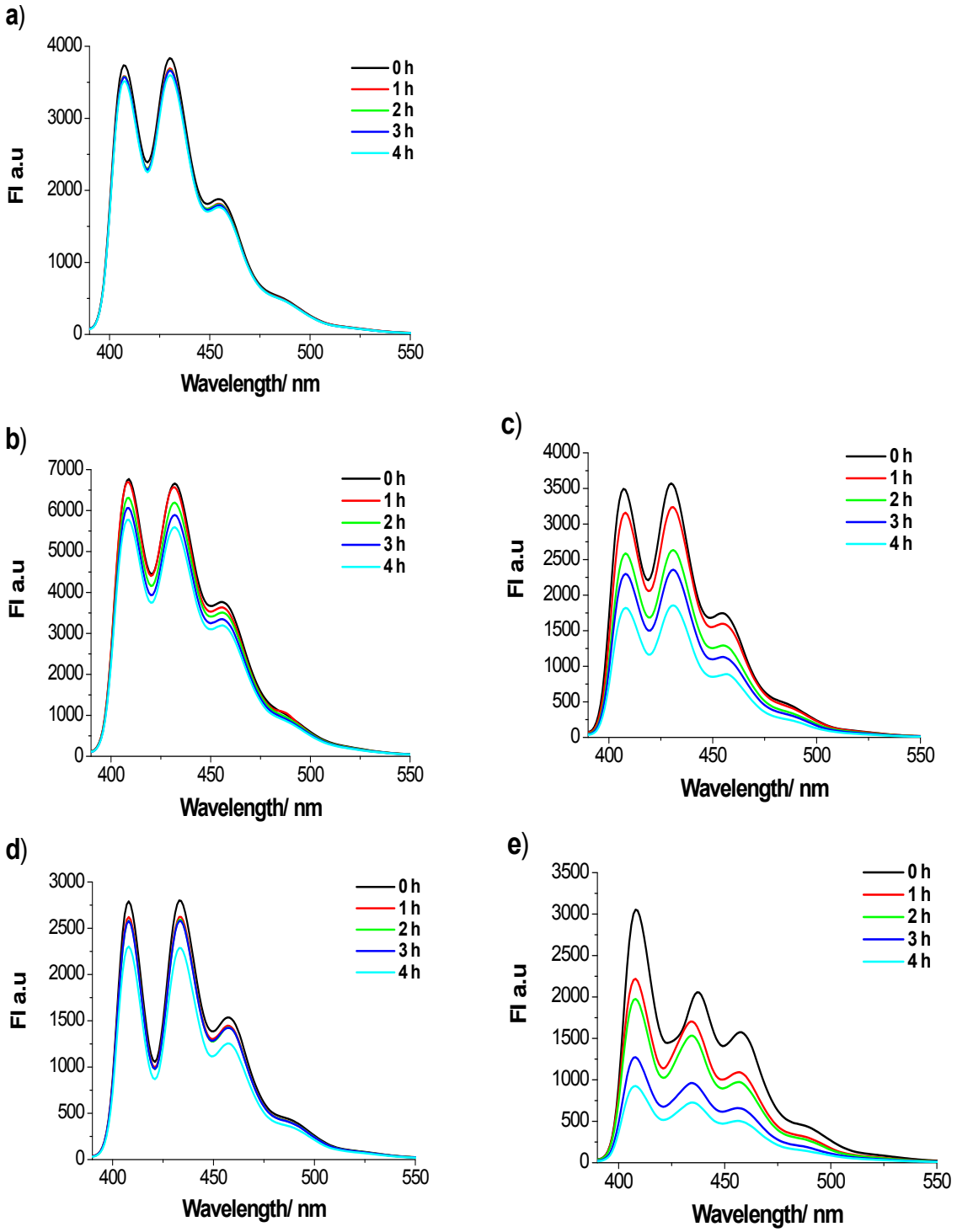

Fig S25. Fluorescence intensity decay of ABMA after irradiation: a) ABMA without porphyrin, b) and c) ABMA with free porphyrin **ATPP-LA** or **ZnTPP-LA** in DMSO at 25 °C, d) and e) with GNP **ATPP-LA-GNP** or **ZnATPP-LA-GNP** in water at 25 °C.

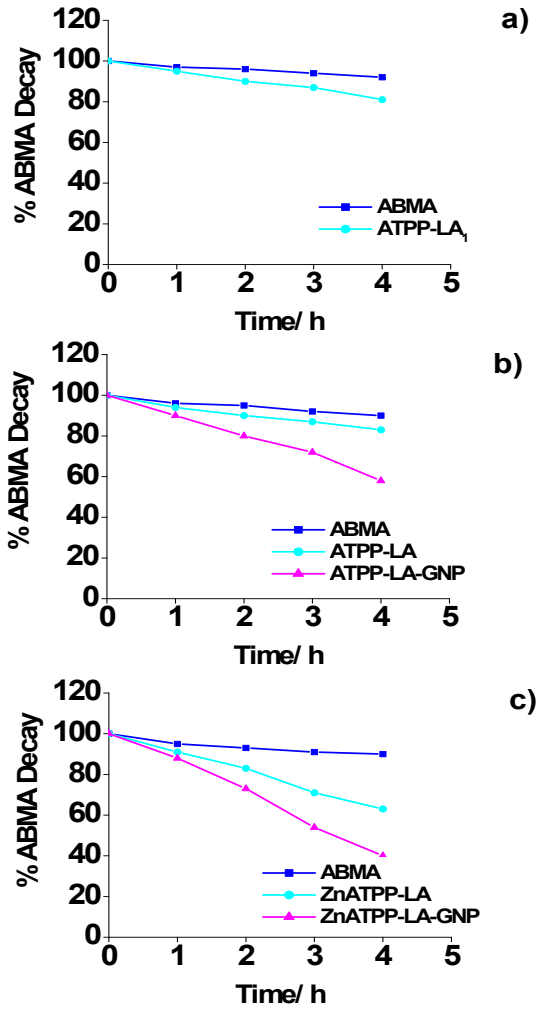

Fig 26. Percentage of fluorescence emission decay of ABMA due to photobleaching. The measures were carried out at 431 nm, in the presence of a) **ATPP-LA$_1$**, b) **ATPP-LA** and **ATPP-LA-GNP**, c) **ZnATPP-LA** and **ZnATPP-LA-GNP**. An ABMA solution without any porphyrin present was used as control. The concentration of porphyrin was 3 μM in all cases.

5) *In vitro* cytotoxicity and internalization studies

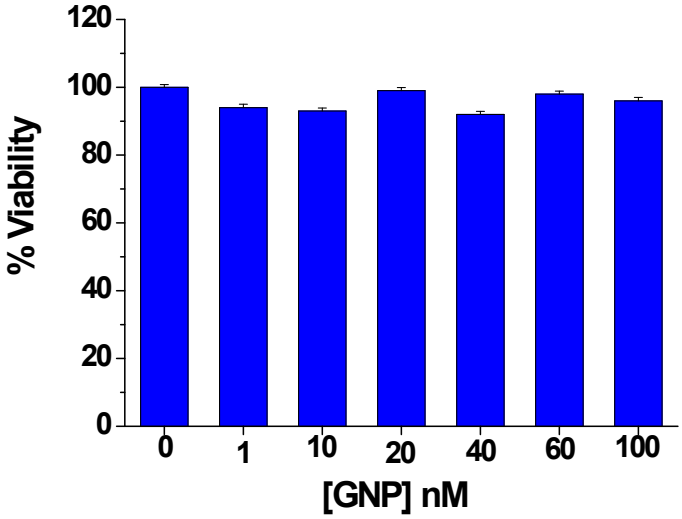

Fig S27. Cytotoxicity data of functionalized GNP with PEG-containing thiol using HeLa cell line. Results displayed as average with error bars corresponding to standard deviation, obtained for n=3 independent experiments.

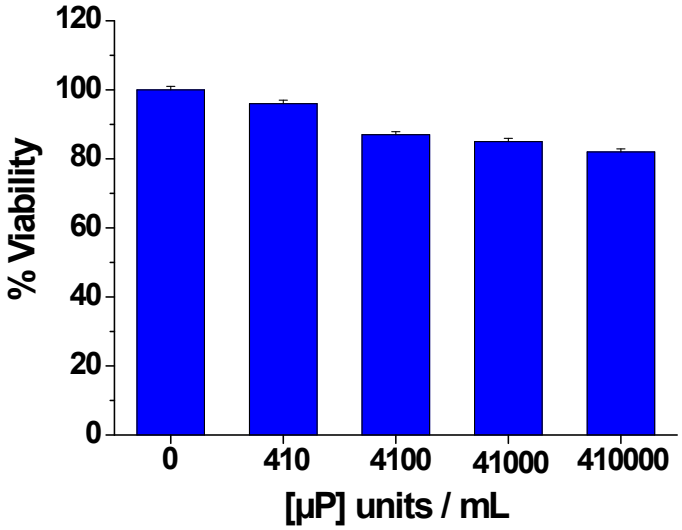

Fig S28. Cytotoxicity data of functionalized µP with PEG-containing thiol using HeLa cell line. Results displayed as average with error bars corresponding to standard deviation, obtained for n=3 independent experiments.

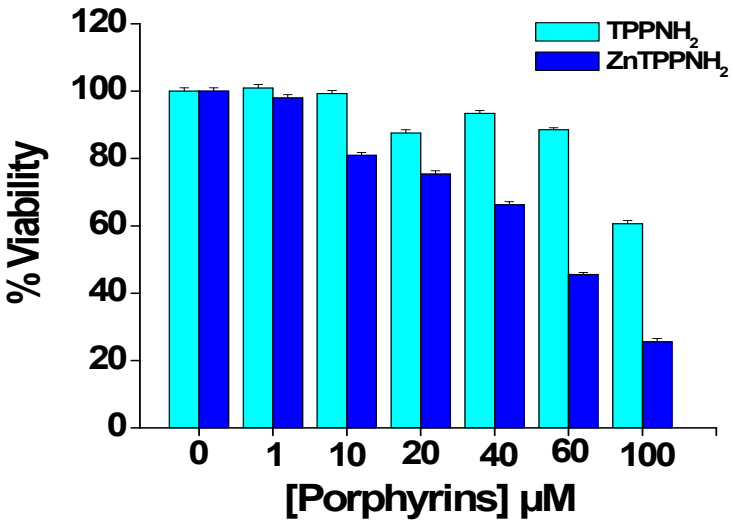

Fig S29. Cytotoxicity data of **TPPNH$_2$** and **ZnTPPNH$_2$** using HeLa cell line. Results displayed as average with error bars corresponding to standard deviation, obtained for n=3 independent experiments.

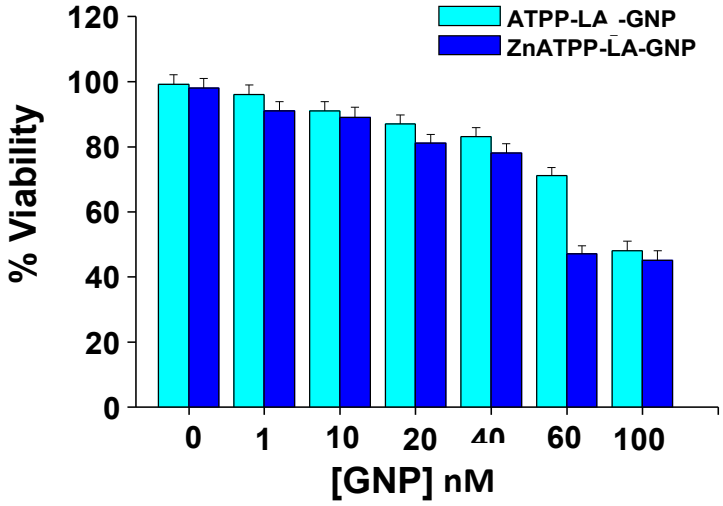

Fig S30. Cytotoxicity data of **ATPP-LA-GNP** and **ZnATPP-LA-GNP** using HeLa cell line. Results displayed as average with error bars corresponding to standard deviation, obtained for n=3 independent experiments.

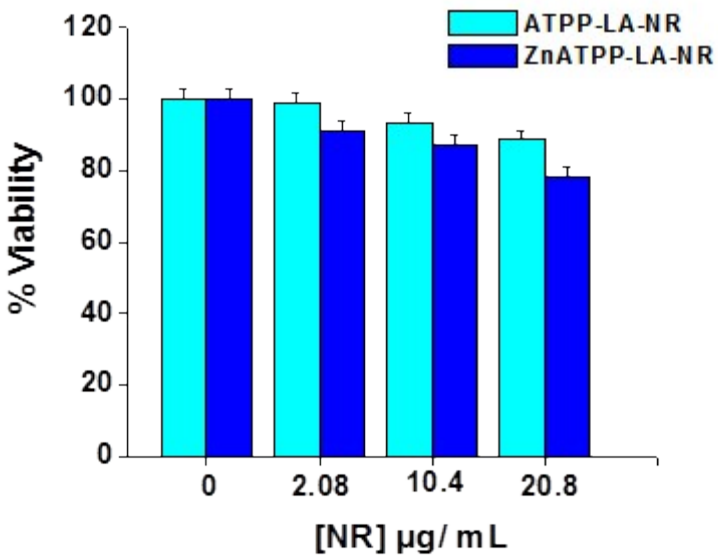

Fig S31. Cytotoxicity data of **ATPP-LA-NR** and **ZnATPP-LA-NR** using HeLa cell line. Results displayed as average with error bars corresponding to standard deviation, obtained for n=3 independent experiments.

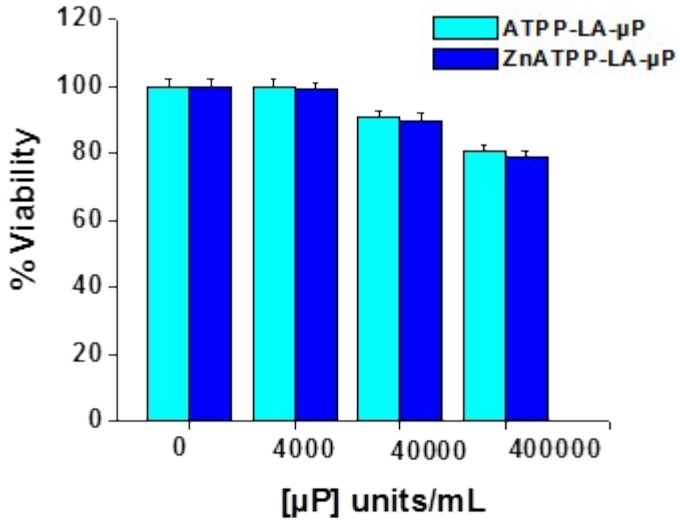

Fig S32. Cytotoxicity data of **ATPP-LA-µP** and **ZnATPP-LA- µP** using HeLa cell line. Results displayed as average with error bars corresponding to standard deviation, obtained for n=3 independent experiments.

References

1 A. D. Adler, F. R. Longo, J. D. Finarelli, J. Goldmacher, J. Assour and L. Korsakoff, *J. Org. Chem.*, 1967, **32**, 476.

2 S. Weimin, S. Qi, W. Yucheng, L. Lihong and T. Jingchao, *J. Heterocycl. Chem.*, 2010, **47**, 1221–1224.

3 W. J. Kruper Jr, T. A. Chamberlin and M. Kochanny, *J. Org. Chem.*, 1989, **54**, 2753–2756.

4 S. U. Hassan, Y. Zhou, L. Zhang, Z. Shi, D. Yang, N. Qu, H. M. Asif and N. Qu, *J.Phys.Chem.C.*, 2016, **120**, 7757–7766.

5 E. Bourlès, R. Alves de Sousa, E. Galardon, M. Selkti, A. Tomas and I. Artaud, *Tetrahedron*, 2007, **63**, 2466–2471.

6 G. I. Giles, K. M. Tasker and C. Jacob, *Free Radic. Biol. Med.*, 2001, **31**, 1279–1283.

7 C. Gispert, A. Serrà, M. E. Alea, M. Rodrigues, E. Gómez, M. Mora, M. L. Sagristá, L. Pérez-García and E. Vallés, *Electrochem. Commun.*, 2016, **63**, 18–21.

8 S. Durán, M. Duch, T. Patiño, A. Torres, O. Penon, R. Gómez-Martínez, L. Barrios, J. Esteve, C. Nogués, L. Pérez-García and J. A. Plaza, *Sensors Actuators B Chem.*, 2015, **209**, 212–224.